

1 **The changing character of twenty-first century precipitation over the**
2 **western United States in the variable-resolution CESM**

3 Xingying Huang, * Paul A. Ullrich

4 *Department of Land, Air and Water Resources, University of California, Davis*

5 *Corresponding author address: Xingying Huang, Department of Land, Air and Water Resources,
6 University of California Davis, Davis, CA 95616.
7 E-mail: xyhuang@ucdavis.edu

ABSTRACT

8 (To be added once the main content settled down)

9 **1. Introduction**

10 There is substantial and growing interest in understanding the character of precipitation within
11 a changing climate, in large part because of the pronounced impacts of water availability on
12 socioeconomic and natural systems (Hegerl et al. 2004; Kharin et al. 2007; Scoccimarro et al.
13 2013). Among these studies, precipitation extremes have been a major focus, particularly drought
14 and flood events (Seneviratne et al. 2012). Studies examining the character of precipitation in a
15 warming world, which utilize models of varying complexity from simple thermodynamic models
16 through complex coupled climate simulations, suggest that although atmospheric water vapor is
17 increasing, the consequences for precipitation are far more complicated. Extreme precipitation
18 events are particularly nuanced: Our best projections suggest that extreme precipitation events
19 will intensify even in regions where mean precipitation decreases (Tebaldi et al. 2006; Kharin
20 et al. 2007).

21 Although future climate projections are subject to large uncertainties, climate models are
22 nonetheless one of the most versatile tools for studying climate variability and extremes events
23 in the future (Easterling et al. 2000). Global climate models (GCMs) have often been used to
24 investigate changes in the mean, variability and extremes of climate, as forced with predicted
25 greenhouse gas (GHGs) concentrations and aerosol emissions (Meehl et al. 2006). Several past
26 studies have investigated global impacts (Seneviratne et al. 2012), but studies addressing impacts
27 at local and regional scales are less common. Although increased GHG concentrations have con-
28 tributed to the observed intensification of heavy precipitation events over the tropical ocean (Allan
29 and Soden 2008) and the majority of Northern Hemisphere overland areas Min et al. (2011), these
30 impacts are much more poorly understood at regional scales due to variability at finer spatial scales
31 associated with the atmospheric circulation (Trenberth 2011). As a consequence of this variability,

³² a confident assessment of changes in regional extremes requires both high spatial resolution and a
³³ long integration period.

³⁴ Insufficient regional-scale climate information has been a major outstanding problem in climate
³⁵ science, as stakeholders and water managers typically require fine-scale information on climate
³⁶ impacts in order to effectively develop adaptation and mitigation strategies. In order to reach the
³⁷ scales needed for effective local planning, dynamical downscaling with regional climate models
³⁸ (RCMs) has been typically used to ascertain the frequency, intensity, and duration of extreme
³⁹ events. By only simulating a limited regional domain, RCMs better capture fine-scale dynami-
⁴⁰ cal features under high horizontal resolution (Bell et al. 2004; Frei et al. 2006; Rauscher et al.
⁴¹ 2010; Wehner 2013). Higher resolution can also enable more accurate simulation of precipitation
⁴² extremes, which can be driven by land use, land/water contrast, snow cover, cloudiness and circu-
⁴³ lation patterns associated with topography (Leung et al. 2003a; Diffenbaugh et al. 2005; Salathé Jr
⁴⁴ et al. 2008; Wehner et al. 2010). Diffenbaugh et al. (2005) studied both heat events and wet events
⁴⁵ over the contiguous United States based on RCMs simulation at 25 km horizontal resolution, and
⁴⁶ demonstrated that fine-scale processes were critical for accurate assessment of local- and regional-
⁴⁷ scale climate change vulnerability. Leung et al. (2003b) showed that the higher-resolution RCMs
⁴⁸ yield more realistic precipitation patterns and produce more frequent heavy precipitation over the
⁴⁹ western U.S. (WUS), consistent with observations.

⁵⁰ Despite their success, RCMs also have known issues associated with inconsistency between the
⁵¹ lateral forcing data and the driven RCM, and the menu of physical parameterizations and param-
⁵² eters typically available to RCMs can lead to over-tuning of the model for a particular geographic
⁵³ region or climatological field (McDonald 2003; Laprise et al. 2008; Mesinger and Veljovic 2013).
⁵⁴ Consequently, there has been growing interest in variable-resolution enabled GCMs (VRGCMs)
⁵⁵ to improve regional climate simulations. Unlike RCMs, which require GCM data to drive the sim-

ulation at lateral boundaries, VRGCMs use a unified model with coarse global resolution and enhanced resolution over a specific study region (Staniforth and Mitchell 1978; Fox-Rabinovitz et al. 1997). VRGCMs have demonstrated comparable utility for regional climate studies at a reduced computational cost, particular when compared to uniform-resolution GCMs (Fox-Rabinovitz et al. 2006; Rauscher et al. 2013).

In this paper, we utilize the recently developed variable-resolution option in the Community Earth System Model (VR-CESM). VR-CESM is based on the CESM (and its predecessor, the Community Climate System Model (CCSM)), a family of models that have been used for decades to study the global climate (Neale et al. 2010a; Hurrell et al. 2013). The overall performance of VR-CESM for modeling regional climate in the California and Nevada is detailed in Huang et al. (2016), where it was argued that VR-CESM has competitive biases in comparison to the Weather Research and Forecasting (WRF) model (a traditional RCM) and the uniform-resolution CESM, when evaluating both against high-quality observations and reanalysis. VR-CESM has been used in a number of studies to capture fine-scale atmospheric processes (Zarzycki et al. 2014, 2015; Rhoades et al. 2015). It was also shown that VR-CESM did not suffer from apparent artifacts within the coarse-fine transition region.

This study focuses on changes in the character of precipitation over the 21st Century within the WUS, as predicted from long-term ensemble runs conducted with VR-CESM with a local grid resolution of $\sim 0.25^\circ$. The WUS is known to be particularly vulnerable to hydrological extreme events, particularly floods and droughts (Leung et al. 2003b; Caldwell 2010), and hosts a variety of local features and microclimates associated with its rough and varied topography. Simulations of the future climate are performed in accordance with the representative concentration pathway (RCP) 8.5 scenario, which describes a “business-as-usual” projection for GHGs (Riahi et al. 2011). RCP8.5 is a baseline scenario with updated base year calibration (to 2005) and no

80 explicit climate policy. In this study we focus on a single RCP since end-of-century projections
81 with the substantially more optimistic RCP2.6 scenario have been found to be qualitatively sim-
82 ilar to mid-century RCP8.5 results (which are assessed in this study). Simulations are further
83 conducted in accordance with the Atmospheric Model Intercomparison Project (AMIP) protocol
84 (Gates 1992), a widely-used approach for climate model diagnosis, validation and intercompari-
85 son that imposes global sea surface temperatures (SSTs) and sea ice. By constraining atmospheric
86 boundary conditions at the sea surface, we avoid model biases that are known to exist in the fully
87 coupled configuration (Grodsky et al. 2012; Small et al. 2014) and accept potential uncertainties
88 associated with our choice of SSTs.

89 Changes in the character of precipitation, in terms of frequency and intensity, have been assessed
90 in our study from recent history through the end of 21st century. A comprehensive set of metrics
91 for precipitation extremes have been evaluated from ensemble simulations over the 26-year peri-
92 ods corresponding to historical (1980-2005), mid-century (2025-2050) and end-of-century (2075-
93 2100). We hypothesize that spatial inhomogeneity in local geography and temperature will also
94 result in similarly inhomogeneous impacts on the precipitation field. We expect that teleconnec-
95 tions (specifically the El Niño-Southern Oscillation, ENSO) will have a pronounced impact on
96 precipitation features over particular area under the changes of mean SST and its variations. Since
97 only one SST dataset was used for this study, we note that our projections are conditioned on a
98 particular future character of ENSO. This is a potentially large source of uncertainty, as at present
99 there is no clear consensus on how ENSO may behave under a warming climate (Fedorov and
100 Philander 2000; Guilyardi et al. 2009), and strengthening or weakening of this pattern will have
101 clear consequences for our results.

102 This work builds on a number of previous studies that have explored the projected future change
103 in WUS precipitation. For example, Kim (2005) applied downscaled climate change signals to se-

104 lected indicators, and concluded that global warming induced by increased CO₂ is likely to drive
105 increases in extreme hydrologic events in the WUS. Duffy et al. (2006) found that mean precip-
106 itation predicted by the RCMs are not statistically significant compared to interannual variability
107 in many regions over WUS, although there is little consistency among the different RCMs as to
108 responses in precipitation to increased GHGs. Gao et al. (2015) pointed out a potentially large
109 increase in atmospheric river events by the end of the 21st century under the RCP8.5 scenario.

110 This paper is structured as follows. Section 2 describes the model setup. Section 3 describes
111 the methodology and reference datasets employed. An assessment of the ability of the model to
112 capture the climatology of the WUS is given in section 4. Results from the future mean climato-
113 logical trend and projected changes to precipitation indices are in section 6. Section 7 summarizes
114 the main points of the study along with further discussion.

115 2. Model Setup

116 CESM is a state-of-the-art Earth modeling framework, consisting of coupled atmosphere, ocean,
117 land and sea ice models (Neale et al. 2010b; Hurrell et al. 2013). In this study, the Community At-
118 mosphere Model version 5 (CAM5) (Neale et al. 2010b) and the Community Land Model version
119 4.0 (Oleson et al. 2010) are used. CAM5 is configured with the Spectral Element (SE) dynamical
120 core, which supports desirable conservation, accuracy and parallel scalability properties (Dennis
121 et al. 2011; Taylor 2011) and incorporates the variable-resolution option (Zarzycki et al. 2014).
122 CLM is employed in the *unigrid* configuration, which allows the land model and atmospheric
123 model to utilize the same model grid so eliminates the need for interpolation. SSTs and sea ice,
124 which are used to compute ocean-atmosphere fluxes, are prescribed in accordance with the AMIP
125 protocol (Gates 1992). The variable-resolution mesh used for this study is depicted in Figure 1, in
126 accord with our past studies (Rhoades et al. 2015; Huang et al. 2016; Huang and Ullrich 2016).

127 Simulations have been performed for the historical period (1979-2005, hereafter referred to as
128 `hist`) and for two future periods: 2024-2050 (hereafter referred to as `mid`) and 2074-2100 (hereafter
129 referred to as `end`). Daily output are recorded for each period on the native SE grid and then
130 remapped to a regional latitude-longitude mesh (??). For purposes of analysis, the first year of
131 each time period was discarded as a spin-up period to allow adequate time for the initialized land
132 and atmosphere to equilibrate. The 26-year duration was chosen to provide an adequate sampling
133 of annual variability for each time phase. As mentioned earlier, GHG concentrations are set based
134 on RCP8.5. Historical SSTs and sea ice are prescribed at 1° resolution, as described by Hurrell
135 et al. (2008). SSTs and sea ice for each future period are developed from fully-coupled RCP 8.5
136 climate simulations with bias correction applied (Cecile Hannay, personal communication). Using
137 prescribed SSTs in place of a coupled ocean model considerably reduces the computation cost and
138 so allows the atmospheric model to be run at a higher overall resolution. Annually-updated land
139 surface datasets, which prescribe land-use characteristics, are interpolated from 0.5° to the land
140 model grid.

141 Ensemble runs are needed to ensure that the sample adequately accounts for climate variability,
142 especially for statistics associated with climatological extremes. However, the exact number of
143 ensemble members required is heavily dependent on the variability of the particular metric being
144 examined, and so no standard ensemble criteria exists. Deser et al. (2012b) suggest that around
145 3 ensemble runs are required to detect a significant epoch difference for JJA (June-July-August)
146 surface temperatures, whereas 10 to 30 ensemble members are needed for that for DJF (Dec.-Jan.-
147 Feb.) precipitation. In our study, the use of prescribed SSTs does reduce the intrinsic variability
148 of the climate system (see supplement), and so we found reasonably converged results with two
149 ensemble members for the historical period and four ensemble members for each future period.

150 **3. Methodology**

151 *a. Precipitation indices*

152 Standard indices have been employed to characterize precipitation (Tebaldi et al. 2006; Zhang
153 et al. 2011; Sillmann et al. 2013). In order to choose a comprehensive (but minimal) set that are
154 informative to stakeholders and water managers, indices from throughout the literature have been
155 assessed. The indices examined include those defined by the Expert Team on Climate Change De-
156 tection and Indices (ETCCDI) (Karl et al. 1999) that are featured in earlier studies (Dulière et al.
157 2011; Sillmann et al. 2013; Diffenbaugh et al. 2005; Singh et al. 2013) and others such as return
158 levels, dry spell and wet spell characteristics defined by either percentiles or by selected thresh-
159 olds. The indices we have chosen for this study attempt to provide a relatively comprehensive
160 characterization of precipitation, and are summarized in Table 1.

161 [Paul: You should probably state at some point why you don't employ drought or dry spell
162 indices]

163 *b. Impacts of ENSO*

164 The impact of ENSO on precipitation is emphasized in our study due to its influence on precipi-
165 tation over a majority of our study area, particularly the southwest U.S. (Cayan et al. 1999; Zhang
166 et al. 2010; Deser et al. 2012a; Yoon et al. 2015). The phase of ENSO (*i.e.* El Niño and La Niña)
167 is identified each year using the Oceanic Niño Index (ONI), defined as the 3-month running means
168 of SST anomalies in the Niño 3.4 region (covering 5N-5S, 120-170W based on NOAA (2013)).
169 An El Niño or La Niña episode is said to occur when the ONI exceeds +0.5 or -0.5 for at least five
170 consecutive months for a water year (*i.e.* from July to June) (NOAA 2013) (see the supplement).
171 In order to adjust for the trend in the SST field associated with climate change, the anomaly is

172 computed against the detrended mean SSTs from the periods 1971-2000, 2020-2050 and 2070-
173 2100 for hist, mid and end respectively, using the aforementioned observed and predicted SST
174 datasets. As argued by Kao and Yu (2009), it may be desirable to use an extended Niño 3.4 region
175 to determine the phase of ENSO – however, when employing SST anomalies integrated over the
176 region 105-170W, we observed no significant impact on ONI statistics.

177 *c. Assessing statistical significance*

178 Student's t-test has been used to test whether or not two datasets at each grid point are statisti-
179 cally equivalent, if the sample population can be adequately described by a normal distribution.
180 The normality of a dataset is assessed under the Anderson-Darling test. When the sample popu-
181 lations do not approximately follow a normal distribution, Mann-Whitney-Wilcoxon (MWW) test
182 is employed in lieu of the t-test. All these tests are evaluated at the 0.05 (α) significance level.
183 When comparing different time periods, statistical tests are conducted using all years from each
184 ensemble run.

185 (add description of the supplement like what are included; see the sst_enso.pdf, mask the land
186 (over land, it should the surface temperature.))

187 *d. Reference datasets*

188 Gridded observational datasets and reanalysis of the highest available quality, with comparable
189 horizontal resolutions to our VR-CESM simulations, are used for assessing the simulation qual-
190 ity. Multiple reference datasets are necessary due to the underlying uncertainty in interpolating
191 precipitation fields. The three datasets employed are as follows:

192 **UW Gridded Data:** The 0.125° UW daily gridded meteorological data is obtained from
193 the Surface Water Modeling group at the University of Washington, covering the period

194 1949-2010 (Maurer et al. 2002; Hamlet and Lettenmaier 2005). The UW dataset imposes
195 topographic corrections by forcing the long-term average precipitation to match that of the
196 PRISM dataset.

197 **National Centers for Environmental Prediction (NCEP) Climate Prediction Center**
198 **(CPC):** This 0.25° daily-output dataset provides gauge-based analysis of daily precipitation
199 from the CPC covering the period 1948-2006. It is a unified precipitation product that cov-
200 ers the Conterminous United States and amalgamates a number of data sources at CPC via
201 optimal interpolation objective analysis.

202 **North American Regional Reanalysis (NARR):** NARR is a ~ 32 km high-resolution reanal-
203 ysis product with 3-hourly output produced by NCEP via dynamical downscaling over North
204 America and covering the period 1979-present (Mesinger et al. 2006).

205 **4. Model Assessment**

206 Before proceeding, we assess the ability of VR-CESM to represent the character of precipitation
207 over the WUS. The indices defined in Table 1 are depicted in Figures 2 and Figure 3 for VR-
208 CESM and each of the reference datasets over the historical period (1980-2005). We assume
209 equal confidence in each of the reference datasets, and use Student's t-test (with UW, CPC and
210 NARR as the three statistical samples) to identify regions where VR-CESM deviates significantly
211 from the reference mean. Regions where differences are statistically significant are identified with
212 stippling in row (a) and (e) of each figure.

213 Compared against the reference, VR-CESM largely captures the spatial patterns of precipitation
214 and its indices. As expected, the majority of precipitation distributed along the northwest coastal

215 area and the mountainous regions of the Cascades and the Sierra Nevada. Nonetheless, several
216 apparent biases are present:

217 First, VR-CESM significantly overestimates Pr over dry regions with deviations between 0.2 mm
218 to 1.5 mm, especially over the eastern flank of the Cascades and on both sides of the Sierra Nevada
219 (with relative differences reaching 50%-150%). As with many regional models, VR-CESM is
220 “dreary” and exhibits too many precipitation days ($R1mm$, $Pr \geq 1$ mm/day and $R5mm$, 1 mm/day \leq
221 $Pr \leq 5$ mm/day) [citation needed]. Nonetheless, over most regions the relative contribution of each
222 precipitation frequency subset to total precipitation ($F1mm$, $F5mm$, $F10mm$, $F20mm$, $F40mm$) is
223 fairly accurate, suggesting that the probability density function describing precipitation intensity
224 is accurately represented almost everywhere.

225 Second, the spatial pattern of precipitation variability agrees well between VR-CESM and ref-
226 erences with agreement everywhere except in the Great Plains (the eastern edge of our domain)
227 and in California’s Central Valley. The Great Plains is not a focus of this study, but the suppressed
228 variance is dominant during the warm season (April-September) and so likely represents a failure
229 of the convection scheme to adequately simulate variability in this region. This bias is also ob-
230 served in 0.25° uniform-resolution CESM simulations [citation needed to ASD data], and so is not
231 a symptom of the eastern edge of the variable-resolution transition region.

232 However, the grossly exaggerated variability over the western flank of the Sierra Nevada through
233 California’s Central Valley does merit some additional discussion. Here, the overestimation of
234 precipitation and enhanced variability is associated with too many extreme precipitation events
235 ($Pr > 20$ mm/day). This bias is related to exaggerated orographic uplift (upslope winds, not shown)
236 and is associated with a dry bias along the eastern flank of the Sierras. Similar biases in simulating
237 extreme precipitation over the topographically complex regions including the Cascades and Sierra
238 Nevada ranges have also been found in high-resolution RCM simulations Walker and Diffenbaugh

239 (2009); Singh et al. (2013), and have been primarily attributed to excessively strong winds. This
240 issue may be further impacted by the diagnostic treatment of precipitation in CAM5 [citation to
241 Morrison Gettleman 1 microphysics].

242 The representation of precipitation in VR-CESM over California was also discussed in Huang
243 et al. (2016), where it was observed that VR-CESM simulations at 0.25° adequately represented
244 regional climatological patterns with high spatial correlation. VR-CESM demonstrated compa-
245 rable performance to WRF at 27 km (which was forced with ERA-Interim reanalysis), but still
246 overestimated overall winter precipitation (by about 25%-35%) compared to reference datasets,
247 with the largest differences over the western edge of the Sierra Nevada. This bias is not allevi-
248 ated by simply increasing the spatial resolution, as experimental VR-CESM simulations at 14km,
249 7km and 3.5km show only modest improvement (Alan M. Rhoades, personal communication).
250 This suggests that the bias might be related with more complex dynamic processes rather than
251 treatment of the orographic effects.

252 CESM at 1° resolution was also assessed in order to better understand the impacts of resolution.
253 We find that precipitation patterns over complex topography are poorly represented and do not
254 capture the spatial patterns induced by orographic effects. Over the Cascades and Sierra Nevada,
255 total precipitation grossly underestimated by 1° CESM, when compared to VR-CESM, gridded
256 and reanalysis datasets (see the supplement [Point to exact figure]). Precipitation has otherwise
257 been smoothed out over the coastal areas and the mountainous regions of the northwest U.S when
258 simulated with CESM at coarse resolution. This result clearly underscores the benefits of high
259 resolution (particularly the representation of topography) in simulating precipitation features. Re-
260 sults are also provided in the supplement for the output from a globally-uniform CESM run at
261 0.25° spatial resolution with the finite volume (FV) dynamical core (Wehner et al. 2014), which
262 exhibits similar performance to VR-CESM (see the supplement [Point to exact figure]). Overall,

263 0.25° resolution appears to provide the best tradeoff between accuracy and computational cost, as
264 coarser resolution does not correctly represent precipitation features and higher resolution does
265 not appear to substantially improve model accuracy.

266 We have also assessed the impact of the ENSO signal within the historical VR-CESM runs by
267 differencing the precipitation fields between the warm phase (i.e. El Niño) and cool phase (i.e.
268 La Niña), compared to references (see the supplement). ENSO exhibits a weaker signal for obser-
269 vational precipitation, compared to VR-CESM, which might suggest that the model exaggerates
270 ENSO's impact on precipitation, especially over the northwest U.S. The improvement of ENSO
271 in the model is directly proportional to the representation of ENSO forced precipitation anomalies
272 (AchutaRao and Sperber 2006).

273 5. Drivers of climatological precipitation change

274 The remainder of this paper now focuses on model predictions of change over the 21st cen-
275 tury. Precipitation has been observed and modeled to be modified in character at both global and
276 regional scales under climate change. The observed intensification of heavy precipitation events
277 over the the recent past for the majority of Northern Hemisphere land areas is primarily attributed
278 to increases in GHGs (Min et al. 2011). GHGs drive radiative changes in the lower troposphere,
279 increase SSTs and lead to increased evaporation, all of which then impact the character of precip-
280 itation events (Allen and Ingram 2002; Sugi and Yoshimura 2004). Several studies have argued
281 that precipitation extremes will intensify continuously through the end of 21st century in both dry
282 and wet regions, although the extent of this change will be spatially heterogeneous (Donat et al.
283 2016).

284 In accordance with the Clausius-Clapeyron (C-C) relationship, saturation vapor pressure in the
285 atmosphere is expected to increase by ~7% for each 1°C increase in temperature (Allan and So-

den 2008). As long as a source of water vapor is present, a corresponding increase in atmospheric water vapor content is expected. Naturally, evaporation over the ocean will increase with climate warming, but increases in water vapor content over land may be constrained by soil moisture (Cayan et al. 2010). When specific humidity is high, heavy rain events become more probable, even if total precipitation is decreasing (Trenberth 2011). This suggests that global total precipitation is expected to increase at a slower rate than precipitation extremes (Allan and Soden 2008).

In accordance with previous studies (e.g. (Allan and Soden 2008; O’Gorman and Schneider 2009; Min et al. 2011)), changes to extreme precipitation follow the C-C relationship more closely than total precipitation amount (Trenberth et al. 2003). However, there is still substantial uncertainty for the magnitude of the change, since precipitation extremes are also dependent on factors such as the vertical velocity profile and temperature (O’Gorman and Schneider 2009).

With overland water vapor constrained by soil moisture content, changes to moderate or heavy precipitation events over the WUS are mainly the result of increased large-scale vapor transport from the eastern Pacific Ocean rather than directly from evaporation, typically associated with atmospheric rivers (ARs) and/or orographic uplift (Trenberth et al. 2003; Neiman et al. 2008). Warming may lead to enhancement of the storm track, which would increase ARs along the U.S. west coast with increased air water vapor content in the future (Dettinger 2011; Gao et al. 2015). In the following sections, both the mean changes of precipitation and distributions of both non-extreme and extreme events are investigated as projected by the VR-CESM model under climate forcing.

The precipitation of the WUS has strong inter-annual variability caused by large-scale atmospheric circulation mainly associated with the ENSO (Leung et al. 2003b). As a significant driver of precipitation, ENSO modulates the storm track behavior over western U.S. with a north-west/southwest precipitation dipole (Gershunov and Barnett 1998), as discussed in d. The pro-

310 jected SSTs we used here states one of the possible cases of ENSO scenarios in the future. How-
311 ever, there is still substantial uncertainty regarding how El Niño will change under global warming
312 (Fedorov and Philander 2000; Guilyardi et al. 2009), which is a source of uncertainty in our results.
313 Capotondi (2013) showed that the diversity of El Niño characteristics in CCSM4 is comparable to
314 what was found in observations, although, as found by Deser et al. (2012c), the overall magnitude
315 of ENSO in CCSM4 [Paul: was this changed at all in CESM1?] is overestimated by 30% over the
316 preindustrial time period.

317 6. Results

318 a. Mean climatology

319 The mean climatological changes in VR-CESM across time periods are depicted in Figure 4.
320 Since the character of WUS precipitation has a strong seasonal contrast, changes to mean precipi-
321 tation, near-surface temperature and near-surface relative humidity are depicted for what we refer
322 to as the cool season (October to March) and the warm season (April to September).

323 As a result of enhanced GHG concentrations, mean annual near-surface temperature ($T_{2\text{avg}}$)
324 increases by about 1.5 to 2 K from hist to mid and about 4 to 6 K from mid to end. Despite the
325 large spatial variation in mean seasonal temperatures, the observed change to mean temperature is
326 fairly uniform, particularly over the ocean and in coastal regions. Away from the coast there is a
327 weak gradient in the temperature change field, with the largest increase in temperatures occurring
328 towards the northeast during the cool season and towards the north during the warm season. The
329 increase in temperature is also about 0.5K and 1.0K larger during the warm season compared to
330 the cool season for mid and end, respectively.

331 Overall, future RH is constrained closely to `hist` since it is governed by competing increases
332 in temperature and atmospheric water vapor content. Although RH increases monotonically over
333 the ocean in response to increased evaporation, over land the character is more heterogeneous: In
334 general, RH tends to increase in regions where $T2\text{avg}$ increase is constrained below ~ 2 K, but
335 decrease when $T2\text{avg}$ anomaly exceeds ~ 2 K. The decrease in these regions is on the order of
336 2% and 3-6%, compared to `mid` and `end` respectively. In fact, trends in RH are spatially consis-
337 tent with temperature increase but opposite in magnitude with a spatial correlation coefficient of
338 approximately 0.8. This suggests that continental evaporation and oceanic water vapor transport
339 are insufficient vapor sources when temperature reaches a certain level, consistent with the obser-
340 vation of Joshi et al. (2008). This effect has also been observed in results by Rowell and Jones
341 (2006) over continental and southeastern Europe and Simmons et al. (2010) over low-latitude and
342 midlatitude land areas.

343 In response to these changes to temperature and RH, from `hist` to `mid` mean precipitation over
344 the entire domain exhibited a 0.2-0.6 mm/day increase during the cool season. The largest changes
345 were over northwest, where cool-season precipitation emerges from large-scale patterns (namely,
346 atmospheric rivers and associated storm systems)(Trenberth et al. 2003; Neiman et al. 2008). Over
347 the warm season, where precipitation in the WUS is primarily from convection, the increase was
348 around 0.2 mm/day through the intermountain west and southwest with drying through the north-
349 west (a decrease in mean precipitation of 0.2 mm/day). These trends largely hold and intensify
350 through the end of century (`end`), except in the intermountain west and southwest regions where
351 precipitation again falls to historical levels. Statistical significance of these results is depicted in
352 Figure 5.

353 The increase in cool season precipitation in the Northwest is largely driven by increased inte-
354 grated vapor transport (IVT) (see Figure 7a). IVT is particularly useful for understanding extreme

355 precipitation events that arise from large-scale meteorological features (Ralph et al. 2004; Leung
356 and Qian 2009; Dettinger 2011). IVT is composed of absolute humidity and wind velocity, which
357 are both impacted by the climate change signal. To understand how these two factors respond
358 to the climate change signal and contribute to the increase in IVT, specific humidity and wind
359 vectors are plotted in Figure 7b. Over the eastern Pacific, we observe increases in both water
360 vapor content and wind speed, which are in turn responsible for increases to IVT in the Pacific
361 Northwest. However, over the continent we see a weakening of the westerlies overland driven
362 by a reduced meridional temperature contrast. The increased cool-season IVT does not manifest
363 strongly along the Pacific coast off of California, where IVT is much smaller on average and is
364 primarily modulated by ENSO.

365 Changes in precipitation over the Intermountain West and Southwest during the warm season are
366 primarily associated with convective processes and so are directly impacted by variations in RH.
367 As shown in Figure 4, RH increases through mid-century in this region (although with modest
368 significance) and then significantly decreases through end-of-century over most the study area
369 (except over where soil moisture was already low in hist). This results in a modest increase in
370 precipitation through mid-century followed by a return to historical precipitation amounts by end-
371 of-century. Further climate warming is expected to further decrease RH and drive increased aridity
372 in this region.

373 *b. Precipitation indices*

374 To see how precipitation changes in a comprehensive way, we have analyzed detailed precipita-
375 tion distributions in order to account for the future changes of different precipitation events, based
376 on our simulation results. The precipitation indices are presented in Table 1. For each index, the
377 changes of precipitation character for each period, averaged over all ensemble members are plotted

378 in Figure 5 (for the indices that quantify precipitation days) and Figure 6 (for the indices describing
379 precipitation amounts). Although mean precipitation shows a weak but overall increasing trend
380 from hist to mid and mid to end (about 10-15%), the precipitation indices exhibit substantially
381 more unique character.

382 When comparing hist to mid, the total rainy days and frequency of non-extreme precipitation
383 have significantly increased (about 10-15%) mainly over the central-east and southeast part of
384 WUS, which is less obvious between mid and end. On the contrary, the frequency of non-extreme
385 precipitation have decreased significantly over the northwest region and the eastern part of the
386 Montana, Wyoming and Oregon from mid to end (about 10%). These changes are the primary
387 driver for the observed change to mean precipitation exhibited in Figure 4.

388 As for extreme precipitation frequency (i.e. days with daily Pr between 10 mm and 40 mm), the
389 number of days increases from hist to mid, but the pattern is scattered over northwest and central
390 WUS. When comparing mid to end, there is a clear and significant increase in extreme precip-
391 itation events over the northwest coastal area (about 20-30%) and eastern flank of the Cascades
392 (larger than 40%). This result is consistent with Dominguez et al. (2012), who observe a robust
393 increase in winter precipitation extremes toward the latter half of the 21st century by an ensemble
394 of RCMs. There is a slight, but insignificant decrease over the Cascades and the Sierra Nevada
395 (significance is low due to the high variability of precipitation). No notable predicted changes have
396 been observed over California.

397 [Paul: For each region it would be extremely valuable to include changes to the return frequency
398 of the most extreme events – i.e. in the Northwest a five-year storm becomes a two-year storm]

399 The associated precipitation signal under a warmer climate is more ambiguous for California
400 (Neelin et al. 2013) considering the extreme variability on interannual time scales (Dettinger
401 2011). Kim (2005) found that under global warming, heavy precipitation events show largest

402 increases in the mountainous regions of the northern California Coastal Range and the Sierra
403 Nevada. However, our results show a minor decrease (though not statistically significant) of ex-
404 treme precipitation over the Sierra Nevada. The decrease over southwest U.S. is mainly due to the
405 intensified La Niña in the future as shown in the Section d.

406 For very extreme precipitation ($\text{Pr} \geq 40 \text{ mm}$) events, there is an increasing trend over the north-
407 west coast (larger than 60%) and the Cascades (about 50%) and its eastern flank (larger than 60%)
408 when comparing hist to end. Significant changes have also observed over the northern moun-
409 tainous part of California for about 20-40% from hist to end. The corresponding changes in rain
410 amount are consistent with the changes of frequency (see Figure 6). Overall, these results indi-
411 cate more extreme precipitation over the northwest U.S with changes in precipitation extremes
412 following more consistently with the C-C relationship.

413 *c. Quantile correlation analysis*

414 To see if changes in mean precipitation can be used to predict changes in extreme precipitation
415 features, the correlations between Pr and specific quantiles have been calculated. Here, selected
416 quantiles including the values at 70% (70p), 80% (80p), 90% (90p), 95% (95p) and 99% (99p)
417 are applied based on the all the daily precipitation data at each grid point within each time period.
418 These quantiles are chosen in order to account for the changes of both moderation and extreme
419 precipitation. The mean Pr and those quantiles for hist, and the differences of these quantities
420 among different time periods can be found in the supplemental figure. Within expectation, regions
421 with higher Pr are associated with larger values of those quantiles, i.e. stronger precipitation
422 extremes. This is further supported by the high correlation (about 0.7-0.9) between Pr and R20mm,
423 R40mm, and Rxmm, not between Pr and non-extreme precipitation events.

424 Spatial correlation is assessed by computing Pearson product-moment coefficient of linear corre-
425 lation between relevant variables. It is found that the absolute changes of Pr in future are positively
426 related with the absolute changes of the quantiles. This relationship is at a moderate level between
427 mid and hist (larger than 0.65), and becomes stronger when going to the end period (reaching
428 ~0.96). Consistently, the mean Pr itself is also positively correlated with the absolute changes of
429 the quantiles in future (around 0.5 to 0.78), except 70p between end and mid and 99p mid and
430 hist.

431 The relative changes of quantiles are also related with the relative changes of Pr with correla-
432 tions around 0.65 to 0.85, except 70p and 80p between end and mid. So, the area featured with
433 higher increase of extreme precipitations in future also tends to have larger increase of its mean
434 precipitation. However, the wetter area does not necessary have more intense changes of moder-
435 ate and extreme precipitation than drier area. **The changes of Pr is not obviously correlated with**
436 **the changes of precipitation indices, which further states that mean precipitation and precipitation**
437 **events undergo different features of changing in the future.**

438 For further investigation of the regional heterogeneity, the frequency distributions of daily rainy
439 days for specific four regions are depicted based on simulation outputs at each gridpoint over
440 26 years of each time period (see Figure 8). We can see over the northwest, Pr intensifies with
441 upper tail going more extreme in the future, especially during end. No notable difference can be
442 observed for California area, except with more extreme upper tail for Pr exceeding 100 mm/day
443 during end, which is due to the increased precipitation extremes over the northern California as
444 shown in Figure 6. Over the inter-mountainous region, similar trends of changes can be seen
445 as the northwest area, with intensified mean and extreme precipitation. For the southwest area,
446 precipitation tends to be more extreme with a moderate level, although no notable difference exists
447 between mid and end.

448 *d. Isolating differences due to climate change and ENSO*

449 The phase of ENSO is well known to have important repercussions on precipitation extremes
450 (Larkin and Harrison 2005; Allan and Soden 2008; Maloney et al. 2014; Yoon et al. 2015). Cai
451 et al. (2014) found a significantly increase for extraordinary precipitation along the eastern Pacific
452 Ocean in the 21st century within the CMIP5 ensemble, associated with increasing frequency of
453 extreme El Niño events due to greenhouse warming. In this part, we will figure out how the ENSO
454 impacts specific regions over our study area, and whether the effects pattern will change over time.

455 ENSO from past to future, the difference of precipitation behaviors between the warm phase (i.e.
456 El Niño) and cool phase (i.e. La Niña) of ENSO is illustrated in Figure 9 for the wet seasons of
457 each time period. Based on the ONI index values, the mean SST anomalies are 1.38, 1.71 and 2.30
458 K during El Niño years, and -1.16, -1.62 and -1.43 K during La Niña years for hist, mid and end
459 respectively. The mean SSTs over the Niño 3.4 region where the are 26.83, 28.62 and 30.54°C
460 for textsfhist, mid and end respectively. Based on the SST datasets we used here, the anomaly
461 of ENSO has intensified. The SST anomalies of each year and each month, and their associated
462 spatial pattern when averaged during the warm and cool phases can be found in the supplement,
463 exhibiting the increasing frequency of El Niño during for mid and almost doubled frequency of La
464 Niña during mid and end compared to the hist.

465 (Huang: As SSTs increase in the future, is not it normal for the anomaly of ENSO to be increased
466 to compensate the changes of water vapor capacity? Might email Neale about this.)

467 During the El Niño phase, intensified mean precipitation is expected over the southwest (Ham-
468 let and Lettenmaier 2007), along with reduced precipitation intensity over the northwest. In La
469 Niña phase, the pattern is essentially reversed, with wetter conditions in the northwest and a drier
470 situation in the Southwest. This feature is characterized as a northwest/southwest precipitation

⁴⁷¹ dipole, triggered by ENSO's modification of the storm track (Gershunov and Barnett 1998; Le-
⁴⁷² ung et al. 2003b), along with modulation of the enhanced precipitation variability (Cayan et al.
⁴⁷³ 1999; Kahya and Dracup 1994). This dipole is also apparently in the frequency of rainy days and
⁴⁷⁴ extreme precipitation events.

⁴⁷⁵ In mid and hist, ENSO is observed to intensify, which appears to be related with the changes
⁴⁷⁶ of the strength of El Niño and La Niña. This can be explained by the SST anomaly magnitude
⁴⁷⁷ (detrended) of warm and cold phases (see the supplement). DeFlorio et al. (2013) also found a
⁴⁷⁸ statistically significant linkages with ENSO and PDO for both the overall and extreme intensity
⁴⁷⁹ of wintertime precipitation over the WUS using CCSM4 (earlier form of CESM). Strengthening
⁴⁸⁰ storm patterns associated with ENSO are also found by Maloney et al. (2014) over California using
⁴⁸¹ CMIP5 output under RCP8.5.

⁴⁸² We have also checked the teleconnection effect of Pacific Decadal Oscillation (PDO) and it
⁴⁸³ did not show strong effect alone. Precipitation features did not change notably when at the cool
⁴⁸⁴ phase or warm phase of PDO during hist. However, together with ENSO at the same phase,
⁴⁸⁵ PDO can have notable effect over northwest. This coupled effect has been found by previous
⁴⁸⁶ studies Gershunov and Barnett (1998), stating ENSO and PDO can "reinforce" each other with
⁴⁸⁷ PDO responding to the same internal atmospheric variability as ENSO (Pierce 2002). **In our**
⁴⁸⁸ **simulations, the patterns of PDO phases differs quite a bit from past to future, though there were**
⁴⁸⁹ **roughly an equal number of positive PDO years and negative PDO years in the data. We suppose**
⁴⁹⁰ **that our 26 years simulation time period might not be long enough to account for the variability of**
⁴⁹¹ **PDO due to its duration for decades. Therefore, in this study, the PDO is not specifically analyzed.**

⁴⁹² The impact of ENSO is further observed by the IVT difference over rainy days between El Niño
⁴⁹³ and La Niña (see Figure 10) accompanying by the wind pattern difference at 850 hPa, showing the

494 increase of the moisture flux for the southwest and decrease for the northwest. This suggests the
495 major role of moisture influx regulation of ENSO.

496 Based on the above results, it can be seen that the magnitude of the effects of ENSO is compara-
497 ble or even higher than the impacts of climate forcing. For further investigation, linear regression
498 is applied to signaling the factor effects due to ENSO and climate forcing. First, we get the SST
499 anomaly of each cool season when ENSO mainly affect followed by the way of Niño 3.4 to be
500 the ENSO factor values. Then, we use the GHGs values at each year to represent the climate
501 forcing factor. The features of the precipitation indices as we defined above are used as response
502 variables. Combined the values of all the time period and all the runs, we got the significance of
503 these two factors' effects at each grid point based on the ANOVA (analysis of variance) output
504 (see the supplement). Changing of the SSTs anomaly can affect most of the study area for non-
505 extreme precipitation events, and southern regions and the Cascades and the Rocky Mountains for
506 precipitation extremes. The GHGs factor mainly shows significant impacts over the northwest and
507 inter-mountainous regions for both non-extreme and extreme precipitation events.

508 We have also examined the linear coefficients of these two factors over where their effects are
509 significant to see the strength that ENSO and GHGs play at each grid point (see the supplement). It
510 is found that the effect of the ENSO is similar to the pattern of the difference between El Niño and
511 La Niña (see Figure 10). In contrast, the effect of the GHGs is close to the pattern of the difference
512 between the different time periods (see Figure 5). We do acknowledge that the values might not be
513 accurate due to the simple linear mode we used here. However, the qualitative conclusions won't
514 change. Therefore, we assume that even the ENSO largely regulates the precipitation over different
515 phases, it won't affect our results shown here for the changes of precipitation features from past to
516 future. Although here is just one of the possible cases of ENSO scenarios in the future, as ENSO

517 behavior is strongly dependent on choice of climate models, the underlying principles should still
518 be consistent.

519 Although, the strength of ENSO intensifies in the future with CESM, there is still substantial
520 uncertainty regarding how El Niño will change under global warming as debated by plenty of
521 studies (Fedorov and Philander 2000; Guilyardi et al. 2009), particularly as ENSO appears to be
522 relatively insensitive to a doubling of CO₂ in most models (DiNezio et al. 2012). Correctly simula-
523 tion changes to the spatial pattern of SSTs ion state-of-the-art coupled GCMs remains challenging
524 Joseph and Nigam (2006); ?); Jha et al. (2014); Taschetto et al. (2014).

525 **7. Discussion and Summary**

526 The increased cool season precipitation extremes tend to result in higher runoff events over
527 the northwest U.S., which are in turn associated with a greater chance of flooding and a loss of
528 snowpack. A decrease in counts of rainy days during the warm season over central and southern
529 California, though small in magnitude, will probably intensify the drought condition due to the
530 deficit of soil moisture with higher evapotranspiration caused by the warmer climate in the future
531 Cayan et al. (2010); Bell et al. (2004).

532 (Huang: Yoon et al. (2015) found a strengthened relation with ENSO for the projected increase
533 in water cycle extremes in California using the output from CESM1 and CMIP5. Similarly by
534 Maloney et al. (2014) using CMIP5 dataset. (check the CESM1?)

535 (Summary is to be added once the main content have been settled down The contribution of
536 human-induced increases in greenhouse gases to the character of precipitation is confounded by
537 patterns of variability in the atmospheric circulation. Consistent with previous studies, changes
538 in more extreme precipitation follow the Clausius-Clapeyron relationship more closely than total
539 precipitation amount. The changes of the strength of ENSO remains uncertain. However, the char-

540 actor of ENSO appears to be the largest factor in understanding changing precipitation extremes
541 in the U.S. West.)

542 *Acknowledgments.* The authors would like to thank Michael Wehner for sharing the dataset and
543 many suggestions. The authors also want to thank Alan M. Rhoades for providing the simulation
544 output. We acknowledge the substantial efforts behind the datasets used in this study, including
545 UW, NCDC and NARR. The simulation data used is available by request at xyhuang@ucdavis.edu.
546 This project is supported in part by the xxx and by the xxx.

547 References

- 548 AchutaRao, K., and K. R. Sperber, 2006: Enso simulation in coupled ocean-atmosphere models:
549 are the current models better? *Climate Dynamics*, **27** (1), 1–15.
- 550 Allan, R. P., and B. J. Soden, 2008: Atmospheric warming and the amplification of precipitation
551 extremes. *Science*, **321** (5895), 1481–1484.
- 552 Allen, M. R., and W. J. Ingram, 2002: Constraints on future changes in climate and the hydrologic
553 cycle. *Nature*, **419** (6903), 224–232.
- 554 Bell, J. L., L. C. Sloan, and M. A. Snyder, 2004: Regional changes in extreme climatic events: a
555 future climate scenario. *Journal of Climate*, **17** (1), 81–87.
- 556 Cai, W., and Coauthors, 2014: Increasing frequency of extreme el niño events due to greenhouse
557 warming. *Nature climate change*, **4** (2), 111–116.
- 558 Caldwell, P., 2010: California wintertime precipitation bias in regional and global climate models.
559 *Journal of Applied Meteorology and Climatology*, **49** (10), 2147–2158.

- 560 Capotondi, A., 2013: Enso diversity in the ncar ccsm4 climate model. *Journal of Geophysical*
561 *Research: Oceans*, **118 (10)**, 4755–4770.
- 562 Cayan, D. R., T. Das, D. W. Pierce, T. P. Barnett, M. Tyree, and A. Gershunov, 2010: Future
563 dryness in the southwest us and the hydrology of the early 21st century drought. *Proceedings of*
564 *the National Academy of Sciences*, **107 (50)**, 21 271–21 276.
- 565 Cayan, D. R., K. T. Redmond, and L. G. Riddle, 1999: ENSO and hydrologic extremes in the
566 western United States*. *Journal of Climate*, **12 (9)**, 2881–2893.
- 567 DeFlorio, M. J., D. W. Pierce, D. R. Cayan, and A. J. Miller, 2013: Western us extreme precipita-
568 tion events and their relation to enso and pdo in ccsm4. *Journal of Climate*, **26 (12)**, 4231–4243.
- 569 Dennis, J., and Coauthors, 2011: CAM-SE: A scalable spectral element dynamical core for the
570 Community Atmosphere Model. *International Journal of High Performance Computing Appli-*
571 *cations*, 1094342011428142.
- 572 Deser, C., R. Knutti, S. Solomon, and A. S. Phillips, 2012a: Communication of the role of natural
573 variability in future north american climate. *Nature Climate Change*, **2 (11)**, 775–779.
- 574 Deser, C., A. Phillips, V. Bourdette, and H. Teng, 2012b: Uncertainty in climate change projec-
575 tions: the role of internal variability. *Climate Dynamics*, **38 (3-4)**, 527–546.
- 576 Deser, C., and Coauthors, 2012c: Enso and pacific decadal variability in the community climate
577 system model version 4. *Journal of Climate*, **25 (8)**, 2622–2651.
- 578 Dettinger, M., 2011: Climate change, atmospheric rivers, and floods in california—a multimodel
579 analysis of storm frequency and magnitude changes1. Wiley Online Library.

- 580 Diffenbaugh, N. S., J. S. Pal, R. J. Trapp, and F. Giorgi, 2005: Fine-scale processes regulate the
581 response of extreme events to global climate change. *Proceedings of the National Academy of*
582 *Sciences of the United States of America*, **102** (44), 15 774–15 778.
- 583 DiNezio, P. N., B. P. Kirtman, A. C. Clement, S.-K. Lee, G. A. Vecchi, and A. Wittenberg, 2012:
584 Mean climate controls on the simulated response of enso to increasing greenhouse gases. *Journal*
585 *of Climate*, **25** (21), 7399–7420.
- 586 Dominguez, F., E. Rivera, D. Lettenmaier, and C. Castro, 2012: Changes in winter precipitation
587 extremes for the western united states under a warmer climate as simulated by regional climate
588 models. *Geophysical Research Letters*, **39** (5).
- 589 Donat, M. G., A. L. Lowry, L. V. Alexander, P. A. OGorman, and N. Maher, 2016: More extreme
590 precipitation in the world [rsquor] s dry and wet regions. *Nature Climate Change*.
- 591 Duffy, P., and Coauthors, 2006: Simulations of present and future climates in the western United
592 States with four nested regional climate models. *Journal of Climate*, **19** (6), 873–895.
- 593 Duli re, V., Y. Zhang, and E. P. Salath  Jr, 2011: Extreme Precipitation and Temperature over the
594 US Pacific Northwest: A Comparison between Observations, Reanalysis Data, and Regional
595 Models*. *Journal of Climate*, **24** (7), 1950–1964.
- 596 Easterling, D. R., G. A. Meehl, C. Parmesan, S. A. Changnon, T. R. Karl, and L. O. Mearns, 2000:
597 Climate extremes: observations, modeling, and impacts. *science*, **289** (5487), 2068–2074.
- 598 Fedorov, A. V., and S. G. Philander, 2000: Is el ni o changing? *Science*, **288** (5473), 1997–2002.
- 599 Fox-Rabinovitz, M., J. C te, B. Dugas, M. D qu , and J. L. McGregor, 2006: Variable resolution
600 general circulation models: Stretched-grid model intercomparison project (SGMIP). *Journal of*
601 *Geophysical Research: Atmospheres (1984–2012)*, **111** (D16).

- 602 Fox-Rabinovitz, M. S., G. L. Stenchikov, M. J. Suarez, and L. L. Takacs, 1997: A finite-
603 difference GCM dynamical core with a variable-resolution stretched grid. *Monthly weather*
604 *review*, **125** (11), 2943–2968.
- 605 Frei, C., R. Schöll, S. Fukutome, J. Schmidli, and P. L. Vidale, 2006: Future change of precipita-
606 tion extremes in Europe: Intercomparison of scenarios from regional climate models. *Journal*
607 *of Geophysical Research: Atmospheres (1984–2012)*, **111** (D6).
- 608 Gao, Y., J. Lu, L. R. Leung, Q. Yang, S. Hagos, and Y. Qian, 2015: Dynamical and thermodynami-
609 cal modulations on future changes of landfalling atmospheric rivers over western north america.
610 *Geophysical Research Letters*, **42** (17), 7179–7186.
- 611 Gates, W. L., 1992: AMIP: The Atmospheric Model Intercomparison Project. *Bulletin of the*
612 *American Meteorological Society*, **73**, 1962–1970.
- 613 Gershunov, A., and T. P. Barnett, 1998: Interdecadal modulation of enso teleconnections. *Bulletin*
614 *of the American Meteorological Society*, **79** (12), 2715–2725.
- 615 Grodsky, S. A., J. A. Carton, S. Nigam, and Y. M. Okumura, 2012: Tropical atlantic biases in
616 ccsm4. *Journal of Climate*, **25** (11), 3684–3701.
- 617 Guilyardi, E., A. Wittenberg, A. Fedorov, M. Collins, C. Wang, A. Capotondi, G. J. Van Olden-
618 borgh, and T. Stockdale, 2009: Understanding el niño in ocean-atmosphere general circulation
619 models. *Bulletin of the American Meteorological Society*, **90** (3), 325.
- 620 Hamlet, A. F., and D. P. Lettenmaier, 2005: Production of Temporally Consistent Gridded Precipi-
621 tation and Temperature Fields for the Continental United States*. *Journal of Hydrometeorology*,
622 **6** (3), 330–336.

- 623 Hamlet, A. F., and D. P. Lettenmaier, 2007: Effects of 20th century warming and climate variability
624 on flood risk in the western us. *Water Resources Research*, **43** (6).
- 625 Hegerl, G. C., F. W. Zwiers, P. A. Stott, and V. V. Kharin, 2004: Detectability of anthropogenic
626 changes in annual temperature and precipitation extremes. *Journal of Climate*, **17** (19), 3683–
627 3700.
- 628 Huang, X., A. M. Rhoades, P. A. Ullrich, and C. M. Zarzycki, 2016: An evaluation of the vari-
629 able resolution-cesm for modeling california's climate. *Journal of Advances in Modeling Earth*
630 *Systems*.
- 631 Huang, X., and P. A. Ullrich, 2016: Irrigation impacts on california's climate with the variable-
632 resolution cesm. *Journal of Advances in Modeling Earth Systems*.
- 633 Hurrell, J. W., J. J. Hack, D. Shea, J. M. Caron, and J. Rosinski, 2008: A new sea surface temper-
634 ature and sea ice boundary dataset for the Community Atmosphere Model. *Journal of Climate*,
635 **21** (19), 5145–5153.
- 636 Hurrell, J. W., and Coauthors, 2013: The community earth system model: A framework for col-
637 laborative research. *Bulletin of the American Meteorological Society*, **94** (9), 1339–1360.
- 638 Jha, B., Z.-Z. Hu, and A. Kumar, 2014: Sst and enso variability and change simulated in historical
639 experiments of cmip5 models. *Climate dynamics*, **42** (7-8), 2113–2124.
- 640 Joseph, R., and S. Nigam, 2006: Enso evolution and teleconnections in ipcc's twentieth-century
641 climate simulations: Realistic representation? *Journal of Climate*, **19** (17), 4360–4377.
- 642 Joshi, M. M., J. M. Gregory, M. J. Webb, D. M. Sexton, and T. C. Johns, 2008: Mechanisms for
643 the land/sea warming contrast exhibited by simulations of climate change. *Climate Dynamics*,
644 **30** (5), 455–465.

- 645 Kahya, E., and J. A. Dracup, 1994: The influences of type 1 el nino and la nina events on stream-
flows in the pacific southwest of the united states. *Journal of Climate*, **7 (6)**, 965–976.
- 646
- 647 Kao, H.-Y., and J.-Y. Yu, 2009: Contrasting eastern-pacific and central-pacific types of enso.
648 *Journal of Climate*, **22 (3)**, 615–632.
- 649
- 650 Karl, T. R., N. Nicholls, and A. Ghazi, 1999: Clivar/gcos/wmo workshop on indices and indicators
for climate extremes workshop summary. *Weather and Climate Extremes*, Springer, 3–7.
- 651
- 652 Kharin, V. V., F. W. Zwiers, X. Zhang, and G. C. Hegerl, 2007: Changes in temperature and
precipitation extremes in the IPCC ensemble of global coupled model simulations. *Journal of*
653 *Climate*, **20 (8)**, 1419–1444.
- 654
- 655 Kim, J., 2005: A projection of the effects of the climate change induced by increased co2 on
extreme hydrologic events in the western us. *Climatic Change*, **68 (1-2)**, 153–168.
- 656
- 657 Laprise, R., and Coauthors, 2008: Challenging some tenets of regional climate modelling. *Meteo-
rology and Atmospheric Physics*, **100 (1-4)**, 3–22.
- 658
- 659 Larkin, N. K., and D. Harrison, 2005: On the definition of el niño and associated seasonal average
us weather anomalies. *Geophysical Research Letters*, **32 (13)**.
- 660
- 661 Leung, L. R., L. O. Mearns, F. Giorgi, and R. L. Wilby, 2003a: Regional climate research: needs
and opportunities. *Bulletin of the American Meteorological Society*, **84 (1)**, 89–95.
- 662
- 663 Leung, L. R., and Y. Qian, 2009: Atmospheric rivers induced heavy precipitation and flooding in
the western US simulated by the WRF regional climate model. *Geophysical research letters*,
664 **36 (3)**.

- 665 Leung, L. R., Y. Qian, and X. Bian, 2003b: Hydroclimate of the western United States based on
666 observations and regional climate simulation of 1981-2000. Part I: Seasonal statistics. *Journal*
667 *of Climate*, **16 (12)**, 1892–1911.
- 668 Maloney, E. D., and Coauthors, 2014: North american climate in cmip5 experiments: part iii:
669 assessment of twenty-first-century projections*. *Journal of Climate*, **27 (6)**, 2230–2270.
- 670 Maurer, E., A. Wood, J. Adam, D. Lettenmaier, and B. Nijssen, 2002: A long-term hydrologically
671 based dataset of land surface fluxes and states for the conterminous United States*. *Journal of*
672 *climate*, **15 (22)**, 3237–3251.
- 673 McDonald, A., 2003: Transparent boundary conditions for the shallow-water equations: testing in
674 a nested environment. *Monthly weather review*, **131 (4)**, 698–705.
- 675 Meehl, G. A., H. Teng, and G. Bannister, 2006: Future changes of el niño in two global coupled
676 climate models. *Climate Dynamics*, **26 (6)**, 549–566.
- 677 Mesinger, F., and K. Veljovic, 2013: Limited area NWP and regional climate modeling: a test
678 of the relaxation vs Eta lateral boundary conditions. *Meteorology and Atmospheric Physics*,
679 **119 (1-2)**, 1–16.
- 680 Mesinger, F., and Coauthors, 2006: North American regional reanalysis. *Bulletin of the American*
681 *Meteorological Society*, **87**, 343–360.
- 682 Min, S.-K., X. Zhang, F. W. Zwiers, and G. C. Hegerl, 2011: Human contribution to more-intense
683 precipitation extremes. *Nature*, **470 (7334)**, 378–381.
- 684 Neale, R. B., and Coauthors, 2010a: Description of the NCAR community atmosphere model
685 (CAM 5.0). *NCAR Tech. Note NCAR/TN-486+ STR*.

- 686 Neale, R. B., and Coauthors, 2010b: Description of the NCAR Community Atmosphere Model
687 (CAM 5.0). NCAR Technical Note NCAR/TN-486+STR, National Center for Atmospheric Re-
688 search, Boulder, Colorado, 268 pp.
- 689 Neelin, J. D., B. Langenbrunner, J. E. Meyerson, A. Hall, and N. Berg, 2013: California winter
690 precipitation change under global warming in the coupled model intercomparison project phase
691 5 ensemble. *Journal of Climate*, **26** (17), 6238–6256.
- 692 Neiman, P. J., F. M. Ralph, G. A. Wick, J. D. Lundquist, and M. D. Dettinger, 2008: Meteorolog-
693 ical characteristics and overland precipitation impacts of atmospheric rivers affecting the west
694 coast of north america based on eight years of ssm/i satellite observations. *Journal of Hydrom-
695 eteorology*, **9** (1), 22–47.
- 696 NOAA, 2013: Defining El Niño and La Niña. Accessed: 2015-
697 08-20, [https://www.climate.gov/news-features/understanding-climate/
698 watching-el-nio-and-la-nia-noaa-adapts-global-warming](https://www.climate.gov/news-features/understanding-climate/watching-el-nio-and-la-nia-noaa-adapts-global-warming).
- 699 O’Gorman, P. A., and T. Schneider, 2009: The physical basis for increases in precipitation ex-
700 tremes in simulations of 21st-century climate change. *Proceedings of the National Academy of
701 Sciences*, **106** (35), 14 773–14 777.
- 702 Oleson, K., and Coauthors, 2010: Technical description of version 4.0 of the Community Land
703 Model (CLM). NCAR Technical Note NCAR/TN-478+STR, National Center for Atmospheric
704 Research, Boulder, Colorado, 257 pp. doi:10.5065/D6FB50WZ.
- 705 Pierce, D. W., 2002: The role of sea surface temperatures in interactions between enso and the
706 north pacific oscillation. *Journal of climate*, **15** (11), 1295–1308.

- 707 Ralph, F. M., P. J. Neiman, and G. A. Wick, 2004: Satellite and caljet aircraft observations of
708 atmospheric rivers over the eastern north pacific ocean during the winter of 1997/98. *Monthly*
709 *Weather Review*, **132** (7), 1721–1745.
- 710 Rauscher, S. A., E. Coppola, C. Piani, and F. Giorgi, 2010: Resolution effects on regional climate
711 model simulations of seasonal precipitation over Europe. *Climate dynamics*, **35** (4), 685–711.
- 712 Rauscher, S. A., T. D. Ringler, W. C. Skamarock, and A. A. Mirin, 2013: Exploring a Global
713 Multiresolution Modeling Approach Using Aquaplanet Simulations. *Journal of Climate*, **26** (8),
714 2432–2452.
- 715 Rhoades, A. M., X. Huang, P. A. Ullrich, and C. M. Zarzycki, 2015: Characterizing Sierra Nevada
716 snowpack using variable-resolution CESM. *Journal of Applied Meteorology and Climatology*,
717 (2015).
- 718 Riahi, K., and Coauthors, 2011: RCP 8.5A scenario of comparatively high greenhouse gas emis-
719 sions. *Climatic Change*, **109** (1-2), 33–57.
- 720 Rowell, D. P., and R. G. Jones, 2006: Causes and uncertainty of future summer drying over europe.
721 *Climate Dynamics*, **27** (2-3), 281–299.
- 722 Salathé Jr, E. P., R. Steed, C. F. Mass, and P. H. Zahn, 2008: A High-Resolution Climate Model
723 for the US Pacific Northwest: Mesoscale Feedbacks and Local Responses to Climate Change*.
724 *Journal of Climate*, **21** (21), 5708–5726.
- 725 Scoccimarro, E., M. Zampieri, A. Bellucci, A. Navarra, and Coauthors, 2013: Heavy precipitation
726 events in a warmer climate: results from CMIP5 models. *Journal of climate*.

- 727 Seneviratne, S. I., and Coauthors, 2012: Changes in climate extremes and their impacts on the
728 natural physical environment. *Managing the risks of extreme events and disasters to advance*
729 *climate change adaptation*, 109–230.
- 730 Sillmann, J., V. Kharin, F. Zwiers, X. Zhang, and D. Bronaugh, 2013: Climate extremes indices
731 in the cmip5 multimodel ensemble: Part 2. future climate projections. *Journal of Geophysical*
732 *Research: Atmospheres*, **118 (6)**, 2473–2493.
- 733 Simmons, A., K. Willett, P. Jones, P. Thorne, and D. Dee, 2010: Low-frequency variations
734 in surface atmospheric humidity, temperature, and precipitation: Inferences from reanalyses
735 and monthly gridded observational data sets. *Journal of Geophysical Research: Atmospheres*,
736 **115 (D1)**.
- 737 Singh, D., M. Tsiang, B. Rajaratnam, and N. S. Diffenbaugh, 2013: Precipitation extremes over the
738 continental United States in a transient, high-resolution, ensemble climate model experiment.
739 *Journal of Geophysical Research: Atmospheres*, **118 (13)**, 7063–7086.
- 740 Small, R. J., and Coauthors, 2014: A new synoptic scale resolving global climate simulation using
741 the community earth system model. *Journal of Advances in Modeling Earth Systems*, **6 (4)**,
742 1065–1094.
- 743 Staniforth, A. N., and H. L. Mitchell, 1978: A variable-resolution finite-element technique for
744 regional forecasting with the primitive equations. *Monthly Weather Review*, **106 (4)**, 439–447.
- 745 Sugi, M., and J. Yoshimura, 2004: A mechanism of tropical precipitation change due to co2
746 increase. *Journal of climate*, **17 (1)**, 238–243.

- 747 Taschetto, A. S., A. S. Gupta, N. C. Jourdain, A. Santoso, C. C. Ummenhofer, and M. H. England,
748 2014: Cold tongue and warm pool enso events in cmip5: mean state and future projections.
749 *Journal of Climate*, **27 (8)**, 2861–2885.
- 750 Taylor, M. A., 2011: Conservation of mass and energy for the moist atmospheric primitive equa-
751 tions on unstructured grids. *Numerical Techniques for Global Atmospheric Models*, Springer,
752 357–380.
- 753 Tebaldi, C., K. Hayhoe, J. M. Arblaster, and G. A. Meehl, 2006: Going to the extremes. *Climatic
754 change*, **79 (3-4)**, 185–211.
- 755 Trenberth, K. E., 2011: Changes in precipitation with climate change. *Climate Research*, **47 (1)**,
756 123.
- 757 Trenberth, K. E., A. Dai, R. M. Rasmussen, and D. B. Parsons, 2003: The changing character of
758 precipitation. *Bulletin of the American Meteorological Society*, **84 (9)**, 1205–1217.
- 759 Walker, M. D., and N. S. Diffenbaugh, 2009: Evaluation of high-resolution simulations of daily-
760 scale temperature and precipitation over the united states. *Climate dynamics*, **33 (7-8)**, 1131–
761 1147.
- 762 Wehner, M. F., 2013: Very extreme seasonal precipitation in the NARCCAP ensemble: model
763 performance and projections. *Climate Dynamics*, **40 (1-2)**, 59–80.
- 764 Wehner, M. F., R. L. Smith, G. Bala, and P. Duffy, 2010: The effect of horizontal resolution
765 on simulation of very extreme US precipitation events in a global atmosphere model. *Climate
766 dynamics*, **34 (2-3)**, 241–247.

- 767 Wehner, M. F., and Coauthors, 2014: The effect of horizontal resolution on simulation qual-
768 ity in the Community Atmospheric Model, CAM5.1. *J. Model. Earth. Sys.*, doi:10.1002/
769 2013MS000276.
- 770 Yoon, J.-H., S. S. Wang, R. R. Gillies, B. Kravitz, L. Hipps, and P. J. Rasch, 2015: Increasing
771 water cycle extremes in California and in relation to ENSO cycle under global warming. *Nature*
772 *communications*, **6**.
- 773 Zarzycki, C. M., C. Jablonowski, and M. A. Taylor, 2014: Using Variable-Resolution Meshes
774 to Model Tropical Cyclones in the Community Atmosphere Model. *Monthly Weather Review*,
775 **142** (3), 1221–1239.
- 776 Zarzycki, C. M., C. Jablonowski, D. R. Thatcher, and M. A. Taylor, 2015: Effects of localized grid
777 refinement on the general circulation and climatology in the Community Atmosphere Model.
778 *Journal of Climate*, **(2015)**.
- 779 Zhang, X., L. Alexander, G. C. Hegerl, P. Jones, A. K. Tank, T. C. Peterson, B. Trewin, and
780 F. W. Zwiers, 2011: Indices for monitoring changes in extremes based on daily temperature and
781 precipitation data. *Wiley Interdisciplinary Reviews: Climate Change*, **2** (6), 851–870.
- 782 Zhang, X., J. Wang, F. W. Zwiers, and P. Y. Groisman, 2010: The influence of large-scale climate
783 variability on winter maximum daily precipitation over North America. *Journal of Climate*,
784 **23** (11), 2902–2915.
- 785 update the mesh grid plot
- 786 update the plot with new label levels

787 LIST OF TABLES

TABLE 1. Precipitation indices employed in this study.

| Name | Definition |
|-------|---|
| Pr | Mean daily precipitation |
| R1mm | Number of days per year with Pr>1 mm |
| SDII | Simple precipitation intensity index: Precipitation amount / $\langle R1mm \rangle$ (mm/day) |
| R5mm | Number of days per year with Pr>1 mm and Pr=<5 mm |
| R10mm | Number of days per year with Pr>5 mm and Pr=<10 mm |
| R20mm | Number of days per year with Pr>10 mm and Pr=<20 mm |
| R40mm | Number of days per year with Pr>20 mm and Pr=<40 mm |
| Rxmm | Number of days per year with Pr>40 mm |
| F1mm | Fraction of precipitation contributed to the total precipitation for days of R1mm (similarly for F5mm, F10mm, F20mm, F40mm and Fxmm) |
| P5mm | Precipitation amount from R5mm (similarly for P10mm, P20mm, F40mm, Pxmm) |

789 LIST OF FIGURES

| | | |
|-----|--|----|
| 790 | Fig. 1. (a) The approximate grid spacing used for the VR-CESM 0.25° mesh. (b) A depiction of 791 the transition from the global 1° resolution mesh through two layers of refinement to 0.25° . 792 (c) Topography height over the study area. | 41 |
| 793 | Fig. 2. Mean precipitation and other related indices from VR-CESM and reference datasets over 794 1980-2005. (Note: Grids with statistically significance difference are marked with stip- 795 pling.) | 42 |
| 796 | Fig. 3. The mean precipitation and other related indices from VR-CESM and reference datasets 797 over 1980-2005 (continued). | 43 |
| 798 | Fig. 4. The mean precipitation (Pr), 2m average temperature ($T2avg$), and 2m relative humidity 799 (RH) averaged over each time period. (Note: Grids with statistically significance difference 800 for the RH are marked with stippling.) | 44 |
| 801 | Fig. 5. Differences of precipitation behaviors from past to future over WUS averaged of each time 802 period. (Note: Grids with statistically significance difference are marked with stippling.) | 45 |
| 803 | Fig. 6. Differences of precipitation behaviors from past to future over WUS averaged of each time 804 period (continued). | 46 |
| 805 | Fig. 7. Changes of specific humidity and horizontal wind pattern at 850hPa for moisture flux il- 806 lustration, and IVT for simulations under different time period of wet season (October to 807 March). (Note: The minimum wind vector is set to be 0.5 m/s, therefore, the wind less than 808 0.5 m/s is also plotted at the minimum length for better visualization.) For all difference 809 plots, make sure to use a common [min,max] range as its currently difficult to tease out dif- 810 ferences. Difference plots should also use a different color table to the mean results (perhaps 811 a single color color table?). | 47 |
| 812 | Fig. 8. Frequency distribution of rainy days ($Pr >= 0.1\text{mm/day}$) over the three time periods from 813 simulations in four regions (with logarithmic vertical scale). (Note: Region 1 to 4 cover 814 Washington and Oregon; California; Nevada, Utah and Idaho; Arizona and New Mexico, 815 respectively.) | 48 |
| 816 | Fig. 9. Difference of precipitation behaviors between warm and cool phases of ENSO from past to 817 future over WUS averaged of each time period. | 49 |
| 818 | Fig. 10. Changes of IVT for simulations under different phases of ENSO of wet season (October to 819 March). (Note: The minimum wind vector is set to be 0.5 m/s, therefore, the wind less than 820 0.5 m/s is also plotted at the minimum length for better visualization.) | 50 |

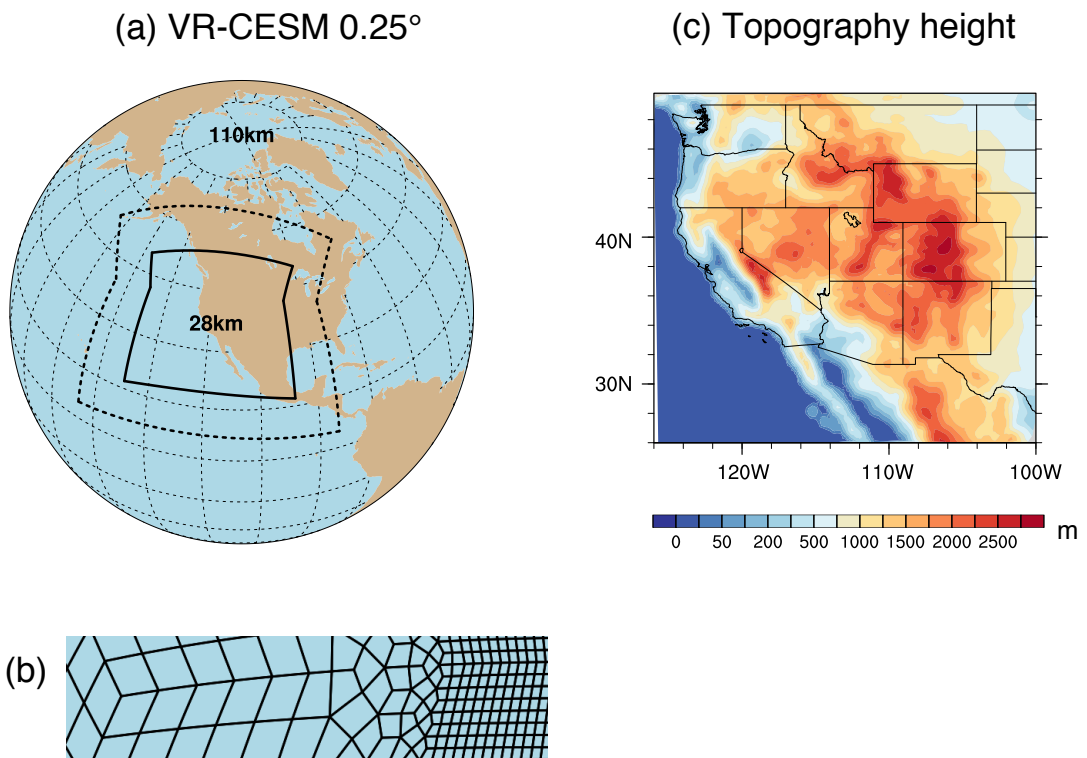
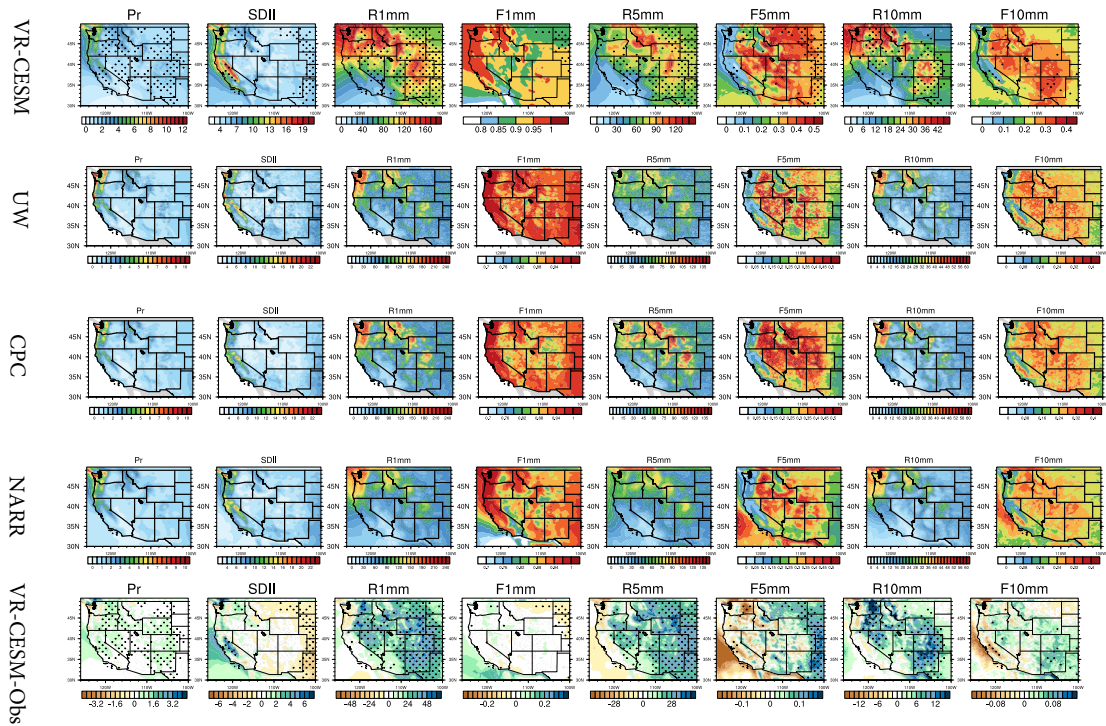
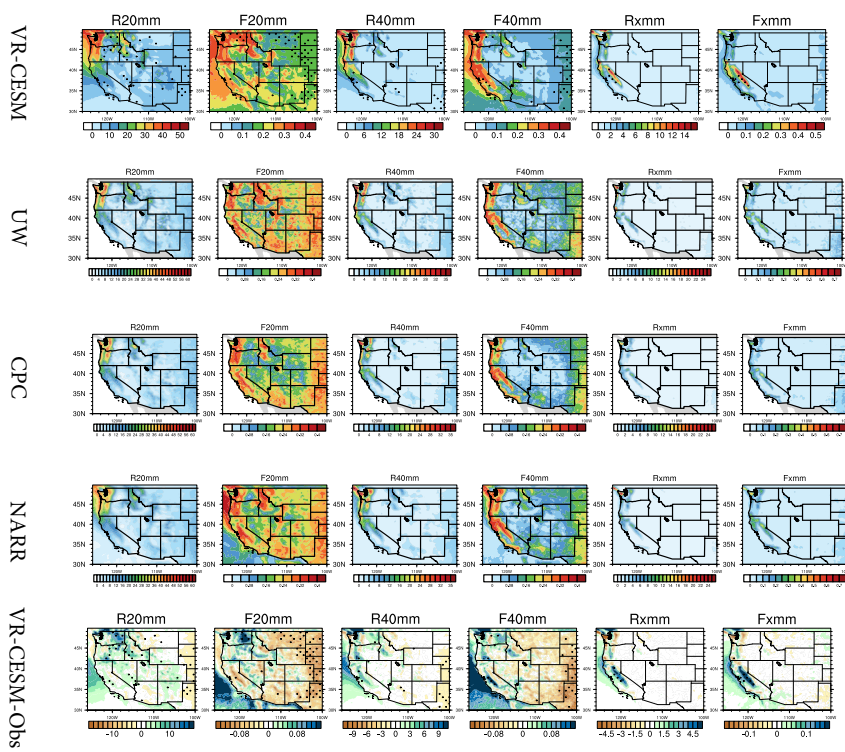


FIG. 1. (a) The approximate grid spacing used for the VR-CESM 0.25° mesh. (b) A depiction of the transition from the global 1° resolution mesh through two layers of refinement to 0.25° . (c) Topography height over the study area.

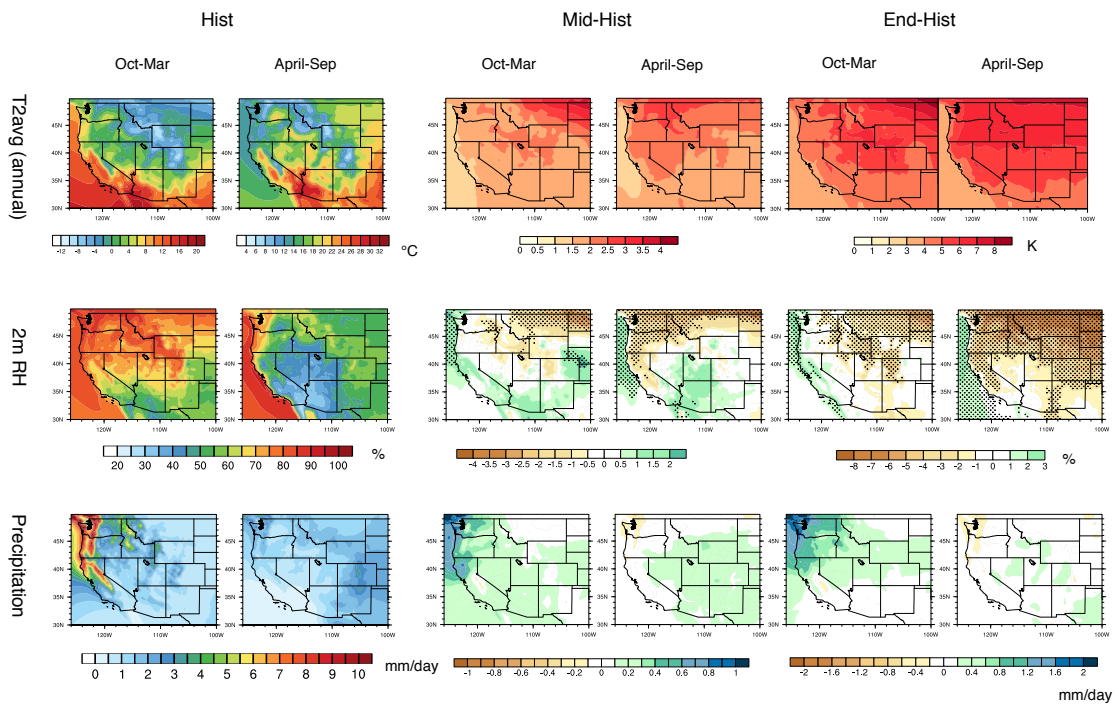


824 FIG. 2. Mean precipitation and other related indices from VR-CESM and reference datasets over 1980-2005.

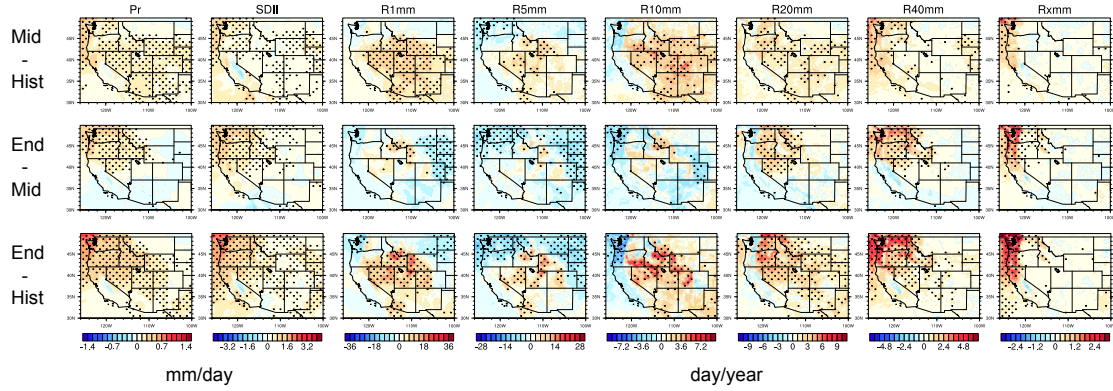
825 (Note: Grids with statistically significant difference are marked with stippling.)



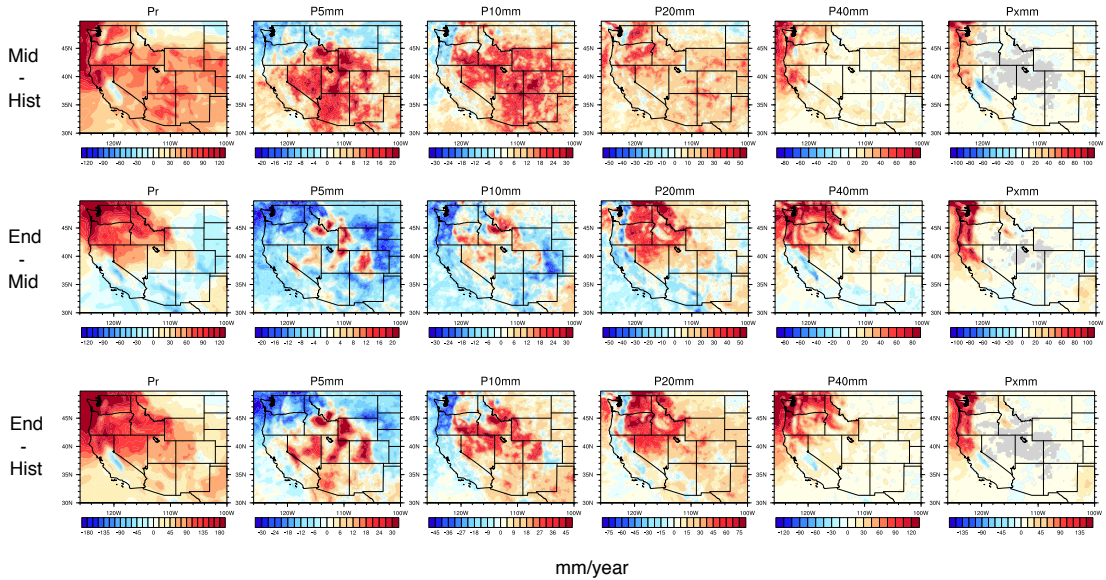
826 FIG. 3. The mean precipitation and other related indices from VR-CESM and reference datasets over 1980-
 827 2005 (continued).



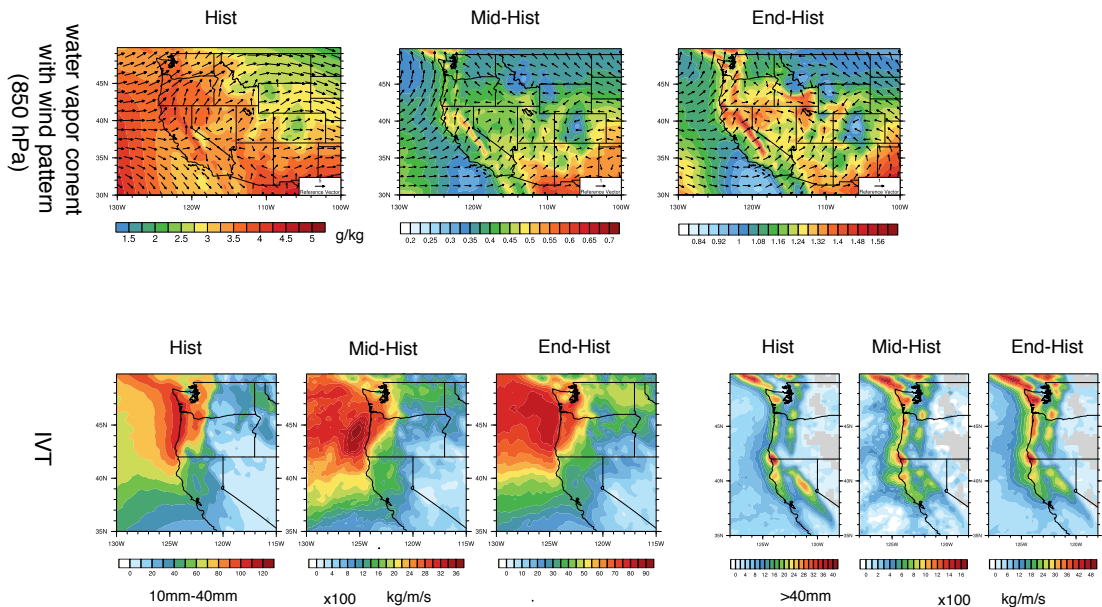
828 FIG. 4. The mean precipitation (Pr), 2m average temperature (T2avg), and 2m relative humidity (RH) aver-
 829 aged over each time period. (Note: Grids with statistically significance difference for the RH are marked with
 830 stippling.)



831 FIG. 5. Differences of precipitation behaviors from past to future over WUS averaged of each time period.
 832 (Note: Grids with statistically significance difference are marked with stippling.)



833 FIG. 6. Differences of precipitation behaviors from past to future over WUS averaged of each time period
 834 (continued).



835 FIG. 7. Changes of specific humidity and horizontal wind pattern at 850hPa for moisture flux illustration, and
 836 IVT for simulations under different time period of wet season (October to March). (Note: The minimum wind
 837 vector is set to be 0.5 m/s, therefore, the wind less than 0.5 m/s is also plotted at the minimum length for better
 838 visualization.) For all difference plots, make sure to use a common [min,max] range as its currently difficult
 839 to tease out differences. Difference plots should also use a different color table to the mean results (perhaps a
 840 single color color table?). 47

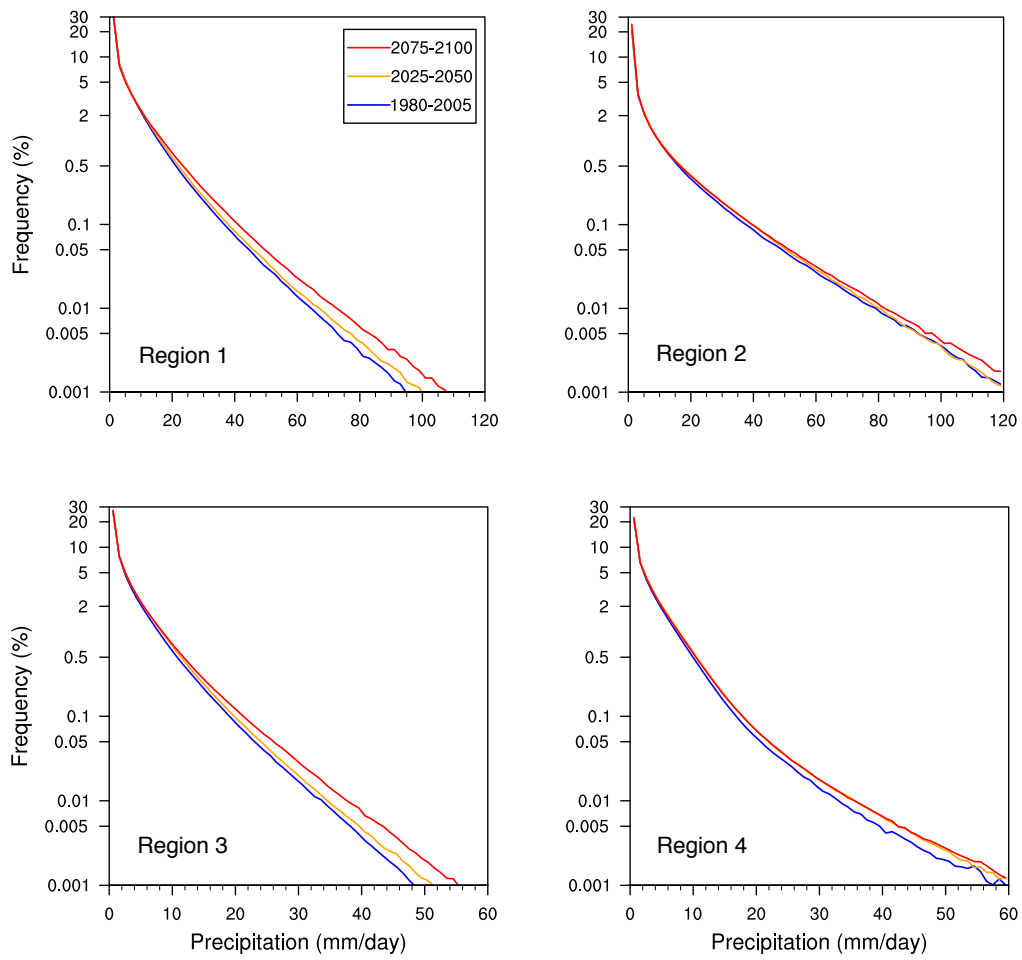
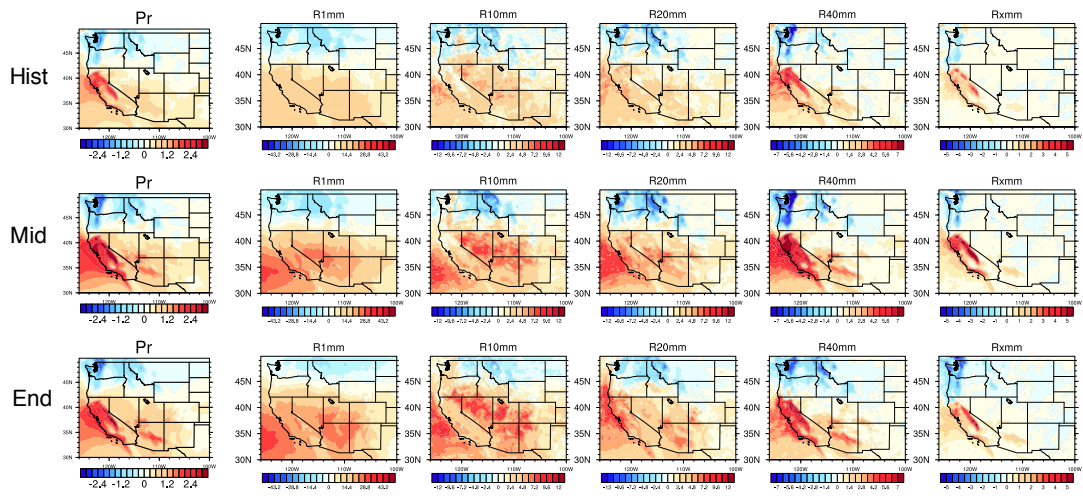
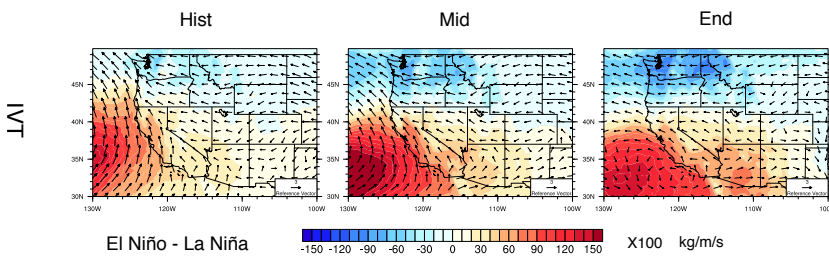


FIG. 8. Frequency distribution of rainy days ($Pr \geq 0.1 \text{ mm/day}$) over the three time periods from simulations in four regions (with logarithmic vertical scale). (Note: Region 1 to 4 cover Washington and Oregon; California; Nevada, Utah and Idaho; Arizona and New Mexico, respectively.)



844 FIG. 9. Difference of precipitation behaviors between warm and cool phases of ENSO from past to future
 845 over WUS averaged of each time period.



846 FIG. 10. Changes of IVT for simulations under different phases of ENSO of wet season (October to March).
 847 (Note: The minimum wind vector is set to be 0.5 m/s, therefore, the wind less than 0.5 m/s is also plotted at the
 848 minimum length for better visualization.)